Eur. Phys. J. B **43**, 363–368 (2005)
DOI: 10.1140/epjb/e2005-00064-0

THE EUROPEAN PHYSICAL JOURNAL B

Dimer site-bond percolation on a square lattice

M. Dolz, F. Nieto, and A.J. Ramirez-Pastor[a]

Departamento de Física, Universidad Nacional de San Luis, CONICET, Chacabuco 917, 5700 San Luis, Argentina

Received 27 August 2004 / Received in final form 6 November 2004
Published online 15 March 2005 –

Abstract. A generalization of the pure site and pure bond percolation problems in which pairs of nearest neighbor sites (site dimers) and linear pairs of nearest neighbor bonds (bond dimers) are independently occupied at random on a square lattice is studied. We called this model as dimer site-bond percolation. Motivated by considerations of cluster connectivity, we have used two distinct schemes (denoted as $S \cap B$ and $S \cup B$) for dimer site-bond percolation. In $S \cap B$ ($S \cup B$), two points are said to be connected if a sequence of occupied sites *and* (*or*) bonds joins them. By using finite-size scaling theory, data from $S \cap B$ and $S \cup B$ are analyzed in order to determine i) the phase boundary between the percolating and non-percolating regions and ii) the numerical values of the critical exponents of the phase transition occurring in the system. The results obtained are discussed in comparison with the corresponding ones for classical monomer site-bond percolation.

PACS. 64.60.Ak Renormalization-group, fractal, and percolation studies of phase transitions – 68.35.Rh Phase transitions and critical phenomena – 05.10.Ln Monte Carlo methods

1 Introduction

The percolation problem has been a focal point of statistical mechanics research for several decades [1–6]. One reason for this current interest is that it is becoming clear that generalizations of the pure percolation problem are likely to have extensive applications in the description of various phenomena in nature. Although it is a purely geometric phenomenon, the phase transition involved in the process can be described in terms of the usual second order phase transition. This mapping to critical phenomena made percolation a full part of the theoretical framework of collective phenomena and statistical physics.

The central idea of the pure percolation theory is based in finding the minimum concentration of elements (sites or bonds) for which a cluster extends from one side to the opposite one of the system. This particular value of the concentration rate is named *critical concentration* or *percolation threshold* and determines a phase transition in the system. Thus, in the random percolation model, a single site (or a bond connecting two sites) is occupied with probability p. For the precise value of p_c, the percolation threshold of sites (bonds), at least one spanning cluster connects the borders of the system (indeed, there exist a finite probability of finding n (> 1) spanning clusters [7–10]). In that case, a second order phase transition appears at p_c which is characterized by well defined critical exponents.

More general percolation problems can be formulated by assuming that both sites and bonds are randomly and independently occupied with occupancy fractions p_s and p_b, respectively. We may then define *site–and–bond* ($S \cap B$) and *site–or–bond* ($S \cup B$) percolation: in $S \cap B$, a cluster is considered to be a set of occupied bonds and sites in which the bonds are joined by occupied sites, and the sites are joined by occupied bonds. $S \cap B$ represents the well-known site-bond percolation, which has many applications in different fields. For instance, it was used to describe the sol-to-gel transition (gelation) of polymers [11]. In this model, bonds represent chemical bonds, occupied sites represent monomers, and empty sites represent solvent molecules. Sites are correlated as in a lattice gas model of a binary mixture. In $S \cup B$, a bond or site contributes to cluster connectivity independently of the occupation of its endpoints.

The phase diagram of the site-bond system in the $p_s - p_b$ parameter space has been widely studied. Thus, the model was mentioned at first by Frisch and Hammersley [12]. Agrawal et al. [13] and Nakanishi and Reynolds [14] showed, by using a series method and position-space renormalization group, respectively, that the critical exponents of pure site percolation are also valid for site-bond percolation. Later, Yanuka and Englman [15] proposed a equation for the critical curve separating the sol-to-gel transition in the site-bond percolation model, for square, triangular, simple cubic and face centered cubic (fcc) lattices. More recently, Tarasevich and van der Marck [16] presented a very complete and systematic study, where site-bond percolation thresholds were calculated by means of numerical simulations in many lattices in two to five dimensions. In addition, the line of

[a] e-mail: antorami@unsl.edu.ar

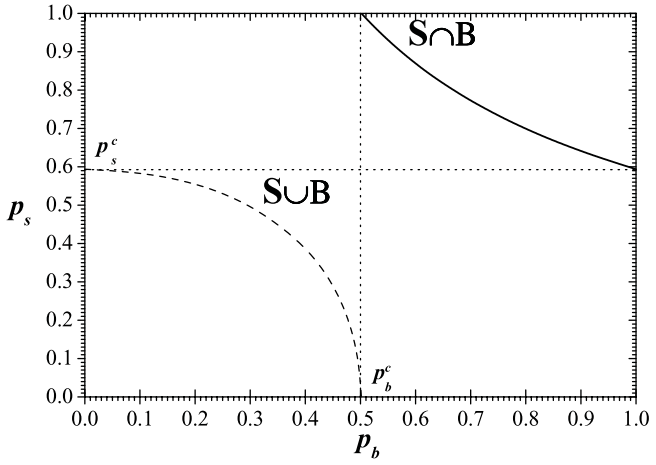

Fig. 1. Typical phase diagram (in the $p_s - p_b$ parameter space) of site-bond percolation ($S \cap B$) and site-or-bond percolation ($S \cup B$) on two-dimensional lattices.

threshold values (critical curve) was parametrized in excellent agreement with the numerical values. A typical phase diagram of site-bond percolation ($S \cap B$) and site-or-bond percolation ($S \cup B$) on two-dimensional lattices is shown in Figure 1. The critical curve corresponding to the $S \cap B$ problem, shown as a solid line, separates the percolating, in which a gel is formed, and the non percolating area, the sol phase. On the other hand, the percolating and the non-percolating region corresponding to the $S \cup B$ problem are separated by the dashed critical curve. Standard site (bond) percolation is recovered as the $p_b = 1$ ($p_s = 1$) case of the $S \cap B$ problem, as well as $p_b = 0$ ($p_s = 0$) case of the $S \cup B$ problem. Note that p_s^c and p_b^c represent the percolation thresholds of standard site and bond percolation, see Figure 1.

Other generalizations of the pure percolation model have been performed by introducing a sort of correlation between the occupation probabilities of adjacent sites and bonds which are usually grouped by the named *correlated percolation*. Among them, one of the most studied is the so-called directed percolation, or percolation with a special direction along which the activity can only propagate one way but not the other [17–21]. In spite of all the differences among generalizations, one common feature remains in most of them: the element deposited occupies only one site (bond) in the lattice. On the contrary, there have been a few studies devoted to generalize the pure percolation model, by including deposition of elements occupying more than one site (bond) [22–29]. Very recently, the pure site and the pure bond percolation of polyatomic species have been studied by using Monte Carlo (MC) simulations [30,31]. In both cases, the dependency of the percolation threshold with the size of the element deposited was discussed.

From an experimental point of view, numerous studies show that on some kinds of metal surfaces, molecular adsorption is the initial step and is followed by dissociation. Among them, the oxidation of carbon monoxide, which is one of the most extensively studied heterogeneous catalysis reactions [32]; the dissociative chemisorption of N_2 on Fe(111) [33], O_2 on Pt(111) [34], O_2 on Ir(111) [35], etc. In all cases, when the diatomic molecule (O_2, N_2) dissociates, it is broken into two monomers, each of which occupies a site. The distributions of such dissociated monomers and the structure of the clusters composed of them are important in the catalytic processes. Because the dimers are randomly placed on the lattice and randomly dissociate, the dissociative adsorption is a spatial random process. Therefore, it can be clearly illustrated by dimer percolation models. In this sense, Gao et al. [29] investigated the process of dissociative adsorption of dimers and studied the percolating properties of the dissociated monomers as a function of both the concentration of dimers and the dissociation probability. A phase diagram separating a percolating from a non-percolating region was obtained.

In all previously mentioned cases, the surface was considered to be chemically homogeneous and smooth. However, i) for many real systems, the most important physical properties depend on the detailed geometry of the substrate, and ii) in contrast to the statistics for the simple particles, the degeneracy of arrangements of dimers is strongly influenced by the structure of the lattice space. Then, it is of interest and of value to inquire how a specific lattice structure influences the main percolation properties of adsorbed dimers. In this sense, the site-bond percolation models may mimic, to a rough approximation, more general heterogeneous surfaces, where some bonds have been removed and the connectivity varies from site to site. In addition, in the best knowledge of the authors, there is still a lack of systematic studies on *site–and–bond* ($S \cap B$) and *site–or–bond* ($S \cup B$) percolation in presence of multiple occupation of sites (bonds).

In this context, the aim of the present paper is (a) to determine, via MC simulations and finite-size scaling theory, the phase diagram in the $p_s - p_b$ space for site dimers and linear bond dimers independently and randomly deposited on a square lattice and (b) to verify the universality class of the phase transition involved in the problem. The proposed system is the simplest model including the essential physics of ($S \cap B$) and ($S \cup B$) percolation with multiple occupation of sites (bonds).

2 The model

Let us consider a periodic square lattice of linear size L on which site dimers and bond dimers are independently deposited at random. The procedure is as follows: 1) a pair of nearest neighbor sites is randomly selected; if it is vacant, the site dimer is then adsorbed on those sites. Otherwise, the attempt is rejected; and 2) a pair of nearest neighbor bonds (aligned along one of the lattice axes) is randomly chosen; if it is vacant, the bond dimer is then dropped onto the lattice. Otherwise, the attempt is rejected. In any case, the procedure is iterated until N_s site dimers and N_b bond dimers are adsorbed and the desired concentrations ($p_s = 2N_s/L^2$, $p_b = N_b/L^2$) are reached.

In the filling process, objects of finite size (dimers) are randomly deposited (irreversibly adsorbed) on an

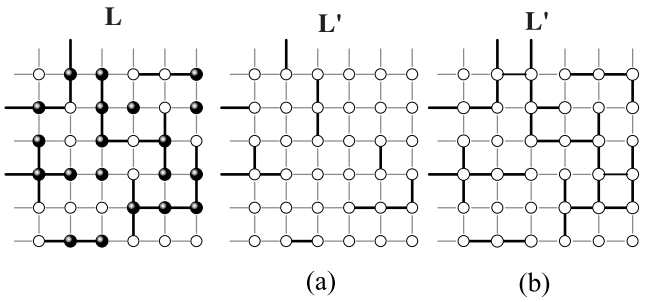

Fig. 2. Rules for the mapping $\mathbf{L} \to \mathbf{L}'$ from an original site-bond lattice $\mathbf{L}$ to an effective bond lattice $\mathbf{L}'$ for a) $S \cap B$ and b) $S \cup B$.

initially empty substrate or lattice with the restriction that they must not overlap with previously added objects. The quantity of interest is the fraction of total site [bond] lattice, $p_s(t)$ $[p_b(t)]$, covered at time t by the deposited objects. Due to the blocking of the lattice by the already randomly adsorbed elements, the limiting or "jamming coverage", $p_s^j = p_s(t = \infty)$ $[p_b^j = p_b(t = \infty)]$, is less than that corresponding to the close packing (p_s^j $[p_b^j] < 1$). Consequently, p_s $[p_b]$ ranges from 0 to p_s^j $[p_b^j]$ for objects occupying more than one site and the total area in the $p_s - p_b$ phase diagram is $p_s^j p_b^j$.

In order to calculate the percolation thresholds, we can now think of a mapping $\mathbf{L} \to \mathbf{L}'$ from the original site-bond lattice $\mathbf{L}$ to an effective bond lattice $\mathbf{L}'$ where each bond and its endpoints sites of $\mathbf{L}$ transforms into an bond one of $\mathbf{L}'$. The rules for the mapping depend on the studied problem. Thus, for *site–and–bond* percolation (see Fig. 2a):

i) each empty bond of $\mathbf{L}$ transforms into an empty one of $\mathbf{L}'$;
ii) each occupied bond with one or two empty endpoint sites of $\mathbf{L}$ transforms into an empty bond in $\mathbf{L}'$; and
iii) each occupied bond with its occupied endpoint sites of $\mathbf{L}$ transforms into an occupied bond of $\mathbf{L}'$.

On the other hand, for *site–or–bond* percolation (see Fig. 2b):

i) each occupied bond of $\mathbf{L}$ transforms into an occupied one of $\mathbf{L}'$;
ii) each empty bond with one or two empty endpoint sites of $\mathbf{L}$ transforms into an empty bond in $\mathbf{L}'$; and
iii) each empty bond with its occupied endpoint sites of $\mathbf{L}$ transforms into an occupied bond of $\mathbf{L}'$.

Once the mapping is completed, we use the standard Hoshen and Kopelman algorithm [36] for studying bond percolation on $\mathbf{L}'$. The percolation threshold in the original and effective lattice must be equal.

3 Finite-size scaling analysis

As the scaling theory predicts [5], the larger the system size to study, the more accurate the values of the threshold obtained therefrom. Thus, the finite-size scaling theory give us the basis to achieve the percolation threshold

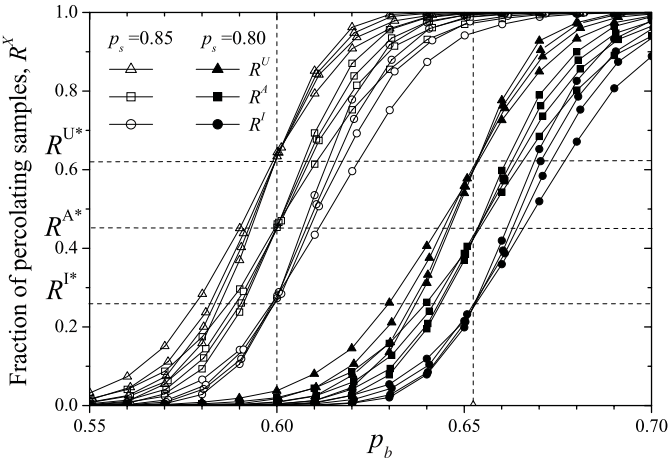

Fig. 3. Fraction of percolating lattices as a function of the concentration p_b. Different criteria, U (triangles), I (circles) and A (squares), are used for establishing the spanning cluster. Open symbols represent curves for $p_s = 0.85$ while filled symbols denote the case $p_s = 0.80$. Horizontal dashed lines show the R^{X^*} universal points. Vertical dashed lines denote the percolation threshold in the thermodynamic limit $L \to \infty$.

and the critical exponents of a system with a reasonable accuracy. For this purpose, the probability $R = R_L^X(p)$ that a lattice composed of $L \times L$ ($2L \times L$) sites (bonds) percolates at concentration p can be defined [2]. Here, as in references [37,38], the following definitions can be given according to the meaning of X: a) $R_L^I(p)$ = the probability of finding a cluster which percolates both in a rightward and in a downward direction; b) $R_L^U(p)$ = the probability of finding either a rightward **or** a downward percolating cluster and c) $R_L^A(p) \equiv \frac{1}{2}\left[R_L^R(p) + R_L^D(p)\right] \equiv \frac{1}{2}\left[R_L^I(p) + R_L^U(p)\right]$.

In the MC simulations, each MC run consists of the following steps: (a) the construction of the lattice for the desired fractions p_s and p_b of site dimers and bond dimers, respectively; (b) the mapping from the original site-bond lattice to the effective bond lattice; and (c) the cluster analysis by using the Hoshen and Kopelman algorithm [36] on the effective bond lattice. In the last step, the existence of a percolating island is verified. This spanning cluster could be determined by using the criteria I, U and A. n runs of such two steps are carried out for obtaining the number m^X of them for which a percolating cluster of the desired criterion X is found. Then, $R_L^X(p_s, p_b) = m^X/n$ is defined and the procedure is repeated for different both values of (p_s, p_b) and lattice sizes. A set of $n = 5 \times 10^4$ independent samples are numerically prepared for each pair (p_s, p_b) and L ($L = 16$, 32, 48, 64, 80, 96, 112). From the point of view of calculations, we set p_s = constant and vary p_b. The critical point corresponding to $p_b = p_b^j$ is obtained for that fixed p_b and variable p_s.

In Figure 3, the probabilities $R_L^I(p_b)$ (circles), $R_L^U(p_b)$ (triangles) and $R_L^A(p_b)$ (squares) are presented for $S \cap B$ percolation and two values of p_s(=0.80 and 0.85). As it can be observed from Figure 3, (a) for a given value of p_s, curves corresponding to different sizes cross each other

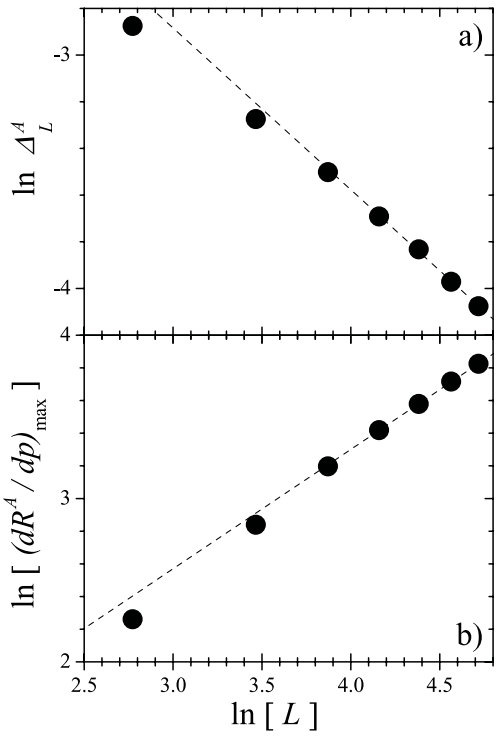

Fig. 4. a) $\ln\left(\Delta_L^A\right)$ as a function of $\ln(L)$. According to equation (1) the slope corresponds to $-1/\nu$. b) $\ln\left(\frac{dR^A}{dp_b}\right)_{max}$ as a function of $\ln(L)$. The slope corresponds to $1/\nu$.

in a unique universal point, R^{X^*}, which depends on the criterion X used and (b) those points are located at very well defined values in the p_b-axes determining the critical percolation threshold for each p_s.

According to the theoretical prediction in reference [2], the critical exponent ν is determined from the divergence of the root mean square deviation of the threshold observed from their average values, Δ_L^X,

$$\Delta_L^X \propto L^{-1/\nu}. \tag{1}$$

As an example of the validity of the last equation, Figure 4a shows Δ_L^A as a function of L (note the log-log scale) for $p_s = 0.8$. According to equation (1), the slope of the line corresponds to $-1/\nu$, being $\nu = 1.38(6)$ in this example.

Another alternative way for evaluating ν is given through the scaling relationship for R^X

$$R^X = \overline{R^X}\left[(p_b - p_b^c)\, L^{1/\nu}\right], \tag{2}$$

being $\overline{R^X}(u)$ the scaling function. Then, the maximum of the derivative of equation (2) leads to $\left(\frac{dR^X}{dp_b}\right)_{max} \propto L^{1/\nu}$.

In Figure 4b we have plotted $\left(\frac{dR^A}{dp_b}\right)_{max}$ as a function of L (note the log-log scale) for different $p_s = 0.8$, whose slope corresponds to $1/\nu$. In this case, $\nu = 1.36(4)$. By using both procedures for different values of p_s and the I, U, A criteria, it can be concluded that the results obtained for ν support the idea that the problem belongs to the same universality class as the random percolation.

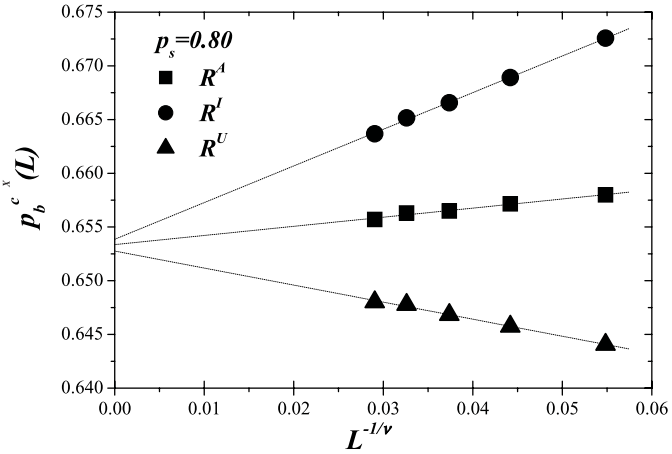

Fig. 5. Extrapolation of p_b^c towards the thermodynamic limit according to the theoretical prediction given by equation (3). Circles, squares and triangles denote the values of $p_b^c(L)$ obtained by using the criteria I, A and U, respectively.

Once ν is known, equation (2) allow for a efficient route to estimate p_b^c from the extrapolation of the positions $p_b^{cX}(L)$ of the maxima of the slopes of $R^X(L)$. For each criterion one expects that [2],

$$p_b^{cX}(L) = p_b^c + A^X L^{-1/\nu} \tag{3}$$

where A^X is a non-universal constant. Figure 5 shows the extrapolation towards the thermodynamic limit of $p_b^{cX}(L)$ according to equation (3) for different criteria. This figure lends support to the assertion given by equation (3): (a) all the curves are well correlated by a linear function, (b) they have a quite similar value for the ordinate in the limit $L \to \infty$ and (c) the fitting determines a different value of the constant A depending of the type of criterion used. It is also important to note that $p_b^{cA}(L)$ gives an almost perfect horizontal line which is a great advantage of the method because it does not require precise values of critical exponent ν in the process of estimating percolation thresholds. The maximum of the differences between $|p_b^{cI}(\infty) - p_b^{cA}(\infty)|$ and $|p_b^{cU}(\infty) - p_b^{cA}(\infty)|$ gives the error bar for each determination of p_b^c.

The scaling law hypothesis also predicts the collapsing of the curves $R_L^X(p_b)$ when they are plotted as a function of a reduced variable $u = (p_b - p_b^c)\, L^{1/\nu}$, see equation (2). Thus, $\overline{R^X}$ is a universal function with respect to the variable u. In Figure 6a this fact is shown for dimers at concentration $p_s = 0.7$ and different values of L as indicated. However, in Figure 6b, R^A is plotted as a function of u for each value of p_s as indicated (each value of p_s is represented by using a different symbol). Similar behavior can be obtained for U and I criteria. Two main conclusions can be drawn from the figure. Namely, a) for a given value of p_s, all the curves used in the experiment (for different values of L) collapse into an universal curve according to the theoretical prediction. This gives an additional proof

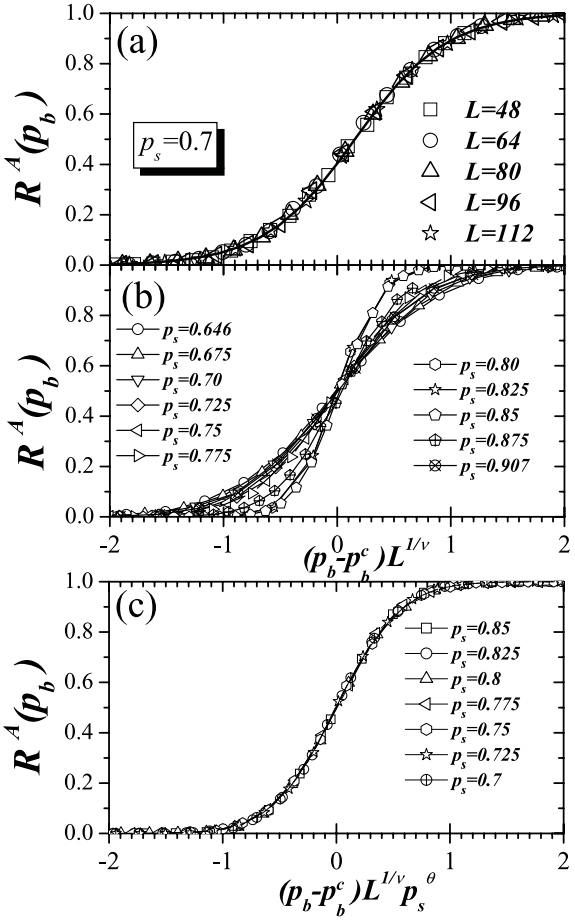

Fig. 6. a) Collapsing plot of the curves for the fraction of percolating samples as a function of $u = (p_b - p_b^c)\, L^{1/\nu}$ for $p_s = 0.7$. Each symbol denotes a different value of L as indicated. b) For each p_s, all the studied lattice sizes (L = 16, 32, 48, 64, 80, 96 and 112) collapse onto a universal curve. The solid lines are simply a guide for the eye. c) The probability R^A as a function of the argument $u' = (p_b - p_b^c)\, L^{1/\nu} p_s^{\theta}$ where the metric factor p_s^{θ} is included in order to collapse all the curves in Figure 6b onto a single one.

for the numerical value of the critical exponent ν. b) $\overline{R^X}$ is not only a function of p_b and L but also of p_s. As it can be seen, the collapsing function is different for each value of p_s considered. This fact determines that the scaling function $\overline{R^X}$ is not an universal function with respect to the variable p_s.

In order to determine the dependence of $\overline{R^X}$ with p_s, the main features of the data shown in Figure 6b have to be considered. As it can be seen, the curves become more steeper upon increasing the value of p_s. In fact, the derivative of the universal function $\overline{R^X}$ with respect to u become more pronounced as p_s increases. Then, it is possible to establish a power law to describe this behavior: $\left(\frac{\partial R^X}{\partial u}\right)_{max} = B p_s^{\lambda}$. On the other hand, the derivatives are narrowed upon increasing p_s. This behavior can also be described by a power law according to $\Delta^X = C p_s^{-\theta}$, being Δ^X the root mean square deviation of $\left(\frac{\partial R^X}{\partial u}\right)$ for each curve.

The maxima of the derivatives (the standard deviation of each derivative) for each value of p_s as a function of p_s can be plotted in a log-log scale (not shown here). The points are very well correlated by a linear function with the fitting parameters $\lambda = 2.03(2)$ and $\theta = 1.98(2)$ and $\lambda = 1.45(2)$ and $\theta = 1.43(2)$ for monomers and dimers, respectively. The number between parenthesis is the error in the determination of the corresponding informed quantities.

According to the equations above, a metric factor might to be included in the scaling function, equation (2), in order to collapse all the curves in Figure 6b onto a single one. Following reference [39], in Figure 6c we plot the probability R^X as a function of the argument $u' = (p_b - p_b^c)\, L^{1/\nu} p_s^{\theta}$. As it is clearly observed, all the curves in Figure 6b collapse onto a single one. It is remarkable that more than 6×10^3 points are included in the collapsing curve. The metric factor introduced here, p_s^{θ}, gives an additional proof for the numerical value of the exponent θ obtained from the behavior of $\Delta^X(p_s)$. A completely similar procedure can be done whether p_b is kept fixed while p_s is varied in the whole range.

4 Phase diagram

The finite-size scaling analysis has been used in the whole range of the variables p_s and p_b in order to determine the percolation thresholds and the phase diagram in the case of dimers. Thus, the resulting $p_s - p_b$ phase diagram for dimer site-bond percolation (full symbols) is shown in Figure 7, in comparison with the standard site-bond percolation for monomers (empty symbols). In the last case, the excellent agreement between our data and previous studies [15,16] (small full squares) supports the applicability of the method used in the present paper.

The main characteristics of the new phase diagram are: 1) the critical curve corresponding to $S \cap B$ model varies between the point $[p_s^j = 0.907(3), p_b = 0.546(2)]$ at left and the point $[p_s = 0.647(2), p_b^j = 0.863(2)]$ at right, where $p_s^j = 0.907(3)$ $[p_b^j = 0.863(2)]$ represents the jamming coverage for site [bond] dimers on square lattice; 2) the critical curve corresponding to $S \cup B$ model varies between the point $[p_s^c = 0.562(3), p_b = 0.0]$ at left and the point $[p_s = 0.0, p_b^c = 0.464(2)]$ at right, where $p_s^c = 0.562(3)$ $[p_b^c = 0.464(2)]$ represents the threshold percolation for site [bond] dimers on square lattice; and 3) the areas of the percolating and non-percolating regions diminish with respect to the corresponding ones for standard site-bond percolation. Thus, the percolating (non-percolating) area changes from 0.1228 (0.2421) for standard site-bond percolation to 0.0450 (0.1951) for dimer site-bond percolation. Then, the effect of dimer site-bond percolation is more pronounced in the case of $S \cup B$ model in comparison with the $S \cap B$ scheme.

5 Conclusions

In this work, the phase diagram of the site-bond percolation problem for dimers is addressed. The influence of

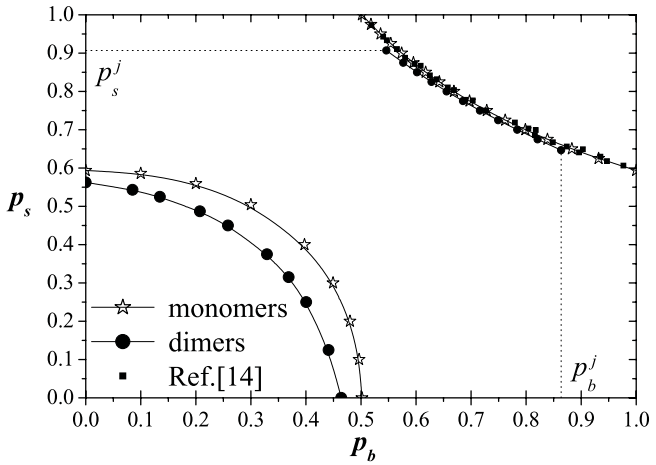

Fig. 7. Phase diagram of dimer site-bond percolation in comparison with the standard site-bond percolation phase diagram on square lattices.

the local correlation introduced by the dimers is more pronounced in the case of $S \cup B$ model in comparison with the $S \cap B$ scheme. The jamming coverage, as it was discussed in the text, fix the limits of the phase diagram curve in the case of $S \cap B$. The percolation thresholds for site (bond) dimers on square lattice denote the limits in the case of $S \cup B$.

In order to test the universality of the problem, the phase transition involved on it has been studied by using finite-size scaling theory. In particular, it was established that (a) if p_b (p_s) remains constant the scaling functions are dependent with respect to the coordinate p_s (p_b) and (b) the problem, in all the studied cases, belongs to the random percolation universality class. The last conclusion can be also confirmed by determining the numerical values of the critical exponents, and the fractal dimension of the spanning cluster.

Finally, the present study encourage us to determine the phase diagram of the site-bond percolation when the size of the percolating species is increased. This work is in progress.

The authors are thankful to Professor G. Zgrablich for the critical reading of the manuscript. This work was made possible by CONICET (Argentina), the Universidad Nacional de San Luis (Argentina) under project 322000 and FUNDACIÓN ANTORCHAS (Argentina).

References

1. J.M. Hammersley, Proc. Cambridge Phil. Soc. **53**, 642 (1957)
2. D. Stauffer, *Introduction to Percolation Theory* (Taylor & Francis, 1985)
3. R. Zallen, *The Physics of Amorphous Solids* (John Willey & Sons, NY, 1983)
4. J.W. Essam, Reports on Progress in Physics **43**, 833 (1980)
5. K. Binder, Reports on Progress in Physics **60**, 488 (1997)
6. C. Lorenz, R. May, R. Ziff, J. Stat. Phys. **98**, 961 (2000)
7. M. Aizenman, Nuclear Phys. B **485**, 551 (1997)
8. J. Cardy, J. Phys. A **31**, L105 (1998)
9. L.N. Shchur, S.S. Kosyakov, Int. J. Mod. Phys. C **8**, 473 (1997)
10. L.N. Shchur, *Incipient Spanning Clusters in Square and Cubic Percolation*, in Springer Proceedings in Physics, Vol. 85, edited by D.P. Landau, S.P. Lewis, H.B. Schuettler (Springer Verlag, Heidelberg, Berlin, 2000)
11. A. Coniglio, H.E. Stanley, W. Klein, Phys. Rev. Lett. **42**, 518 (1979)
12. H.L. Frisch, J.M. Hammersley, J. Soc. Ind. Appl. Math. **11**, 894 (1963)
13. P. Agrawal, S. Render, P.J. Reynolds, H.E. Stanley, J. Phys. A: Math. Gen. **12**, 2073 (1979)
14. H. Nakanishi, J. Reynolds, Phys. Lett. **71** A, 252 (1979)
15. M. Yanuka, R. Englman, J. Phys. A: Math. Gen. **23**, L339 (1990)
16. Y.Y. Tarasevich, S.C. van der Marck, Int. J. Mod. Phys. C **10**, 1193 (1999)
17. W. Kinzel, *Directed Percolation*, in Percolation Structures and Processes, edited by G. Deutscher, R. Zallen, J. Adler (Hilger, Bristol, 1983)
18. P. Grassberger, A. de la Torre, Ann. Phys. N.Y. **122**, 373 (1979)
19. P. Grassberger, K. Sundermeyer, Phys. Lett. B **77**, 220 (1978)
20. K. De'Bell, J.W. Essam, J. Phys. A: Math. Gen. **18**, 355 (1985)
21. A. Tretyakov, N. Inui, J. Phys. A: Math. Gen. **28**, 3985 (1995)
22. J.W. Evans, D.E. Sanders, Phys. Rev. B **39**, 1587 (1989)
23. H. Harder, A. Bunde, W. Dieterich, J. Chem. Phys. **85**, 4123 (1986)
24. H. Holloway, Phys. Rev. B **37**, 874 (1988)
25. M. Henkel, F. Seno, Phys. Rev. E **53**, 3662 (1996)
26. E.L. Hinrichsen, J. Feder, T. Jossang, J. Stat. Phys. **44**, 793 (1986)
27. Y. Leroyer, E. Pommiers, Phys. Rev. B **50**, 2795 (1994)
28. B. Bonnier, M. Honterbeyrie, Y. Leroyer, C. Meyers, E. Pommiers, Phys. Rev. B **49**, 305 (1994)
29. Z. Gao, Z.R. Yang, Physica A **255**, 242 (1998)
30. V. Cornette, A.J. Ramirez-Pastor, F. Nieto, Physica A **327**, 71 (2003)
31. V. Cornette, A.J. Ramirez-Pastor, F. Nieto, Eur. Phys. J. B **36**, 391 (2003)
32. R.M. Ziff, E. Gulari, Y. Barshad, Phys. Rev. Lett. **56**, 2553 (1986), and references therein
33. C.T. Rettner, H. Stein, Phys. Rev. Lett. **59**, 2768 (1987)
34. C.T. Rettner, C.B. Mullins, J. Chem. Phys. **94**, 1626 (1991)
35. J.E. Davis, P.D. Nolan, S.G. Karseboom, C.B. Mullins, J. Chem. Phys. **107**, 943 (1997)
36. J. Hoshen, R. Kopelman, Phys. Rev. B **14**, 3438 (1976); J. Hoshen, R. Kopelman, E.M. Monberg, J. Stat. Phys. **19**, 219 (1978)
37. F. Yonezawa, S. Sakamoto, M. Hori, Phys. Rev. B **40**, 636 (1989)
38. F. Yonezawa, S. Sakamoto, M. Hori, Phys. Rev. B **40**, 650 (1989)
39. V. Privman, P.C. Hohenberg, A. Aharony, *"Universal Critical-Point Amplitude Relations"*, in Phase Transitions and Critical Phenomena, edited by C. Domb, J.L. Lebowitz, Vol. 14, Chap. 1 (Academic, NY, 1991), pp. 1134 and 364367